

Preparation of biomimetic membrane with hierarchical structure and honeycombed through-hole for enhanced oil–water separation performance

Shuai Luo, Xueyan Dai, Yanlong Sui, Peihong Li, Chunling Zhang*

School of Materials Science and Engineering, Jilin University, Changchun, 130022, PR China

ARTICLE INFO

Keywords:

Electrospray
Polydimethylsiloxane
Honeycombed through-hole

ABSTRACT

Efficient oil–water separation plays a vital role in treating large amounts of industrial wastewater. However, current traditional separation methods are entwined with problems such as low efficiency and poor operability. Herein, we reported a nanofiber based on electrospinning and electro-spray technology and spraying microspheres on the surface of a fiber mat for efficient oil–water separation. Owing to the electrostatic repulsion among the microspheres, the surface of the developed membrane had a honeycomb-like through-hole structure and super-high oil–water separation efficiency and oil flux. After 10 cycles, the membrane showed good separation efficiency and flux. This innovative work may provide a new idea and method for the design of biomimetic biopolymers, with broad application prospects in the field of oil–water separation.

1. Introduction

Since the 20th century, global industries have continued to prosper because of the rapid development of science and technology. At the same time large amounts of industrial oily wastewater are discharged everywhere, inflicting catastrophic damage to the ecosystem and human health [1–3]. Accordingly, the recovery of water that has been contaminated by oil is important. Traditional oil–water separation methods such as the use of gravity, mechanical equipment (e.g., boom, oil skimmer, etc.), air flotation, adsorption, and biodegradation have low separation efficiency, high operating cost, heavy equipment, and other problems [4–7]. In some cases, these separation methods difficultly recover oil solvents and have poor recycling rates, which may cause secondary pollution to water bodies [8,9]. Thus, it was very urgent to treat a large amount of industrial oily wastewater.

Membrane-separation technology is regarded as the most promising oil–water separation method owing to its high separation efficiency, simple operation, and low energy consumption [10–12]. The efficiency of oil–water separation depends on the membrane hydrophobicity and lipophilicity [4], and the former depends on low surface energy and surface roughness [13,14]. Inspired by lotus leaves and rose petals, microprotrusions formed by constructing micro-nano-hierarchical structures can render a surface super-hydrophobic [15,16]. The rough surface can trap air on the surface of the droplet and membrane to reduce the contact area, thereby achieving super-hydrophobic

properties. Many techniques have been successfully used to construct super-hydrophobic rough surfaces [2,17–20]. Among these technologies, electrospinning is extensively used due to its low cost, simple device, and controllable process [21–23]. Recent studies have shown that the effective combination of electrospinning and electro-spraying technologies can produce excellent and recyclable oil–water separation membranes [24,25]. Moreover, other researchers have attempted to add hydrophobic functional groups to the membrane surface to reduce surface energy [26]. Among them, the application of nanomaterials or chemical substances with long fluoroalkyl chains is a useful method, but it is accompanied with environmental-pollution problems [27,28].

Polydimethylsiloxane (PDMS), a fluorine-free polymer, is suitable for making various hydrophobic membranes owing to its low surface energy. It is also extensively used to form hydrophobic surfaces in other fields [29,30]. However, the use of PDMS to prepare oil–water separation membranes is limited by its low molecular weight. In the present study, we assumed that the copolymerization of rigid groups and flexible polymers can lead to the formation of a controllable honeycomb structure during electro-spraying. In the present study, we used hydrosilation to introduce the benzene-ring structure into polysilane. PDMS with different rigid-flex section ratios was synthesized and mixed with poly(vinylidene fluoride) (PVDF). Electro-spray technology was further used to form microstructures on pure PVDF membrane to obtain a hierarchical structure. The prepared layered structure membrane was expected to show excellent oil–water separation performance, thereby

* Corresponding author.

E-mail address: clzhang@jlu.edu.cn (C. Zhang).

<https://doi.org/10.1016/j.polymer.2021.123522>

Received 9 December 2020; Received in revised form 6 February 2021; Accepted 8 February 2021

Available online 12 February 2021

0032-3861/© 2021 Elsevier Ltd. All rights reserved.

providing a new method for preparing new oil–water separation membranes.

2. Experimental

2.1. Materials

4,4'-dihydroxydiphenyl, potassium carbonate (K_2CO_3), allyl bromide, octamethylcyclotetrasiloxane (D4), dimethyldichlorosilane, Karstedt's catalyst solution, and 1,1,3,3-tetramethyldisiloxane (TMDS) were purchased from Macklin Industrial Corporation, China. PVDF (Solef 6010; $M_w = 600\,000\text{ g mol}^{-1}$) was obtained from Solvay Advanced Polymers L.L.C (Alpharetta, GA, USA). Kg-23 chain extender was obtained from Mendeleyev University of Chemical Technology, Russia. Toluene, anhydrous magnesium sulfate, magnesium sulfate anhydrous, dimethylformamide (DMF), acetone, tetrahydrofuran (THF), anhydrous calcium chloride, anhydrous calcium chloride, and anhydrous ethanol were obtained from Beijing Chemical Industry, Beijing, China. Distilled water obtained with a laboratory water-purification system (Smart-Q15 Shanghai Hitech Instruments Co., Ltd., China) was used throughout. All solvents were used as received without further purification.

2.2. Characterization techniques

1H NMR spectra were obtained using a nuclear magnetic resonance (NMR) spectrometer (Avance 600, Bruker) with $CDCl_3$ as solvent and tetramethylsilane as an internal reference. Fourier transform infrared (FT-IR) spectra were obtained with an FT-IR system (Nexus 670, Nicolet) within the range of $4000\text{--}400\text{ cm}^{-1}$ at room temperature. The samples were mixed with KBr and pressed into flasks. The morphologies and microspheres of the copolymer were observed with a scanning electron microscopy (SEM, FEI XI, 30 ESEM FEG), and the elemental composition of the copolymer membranes was characterized using an energy-dispersive spectrometer (EDS, EDAX Genesis XM2) connected to the SEM. Water contact angles were obtained with a Drop Shape Analyzer (DSA100, Kruss). Droplets of deionized water from a $4\text{ }\mu\text{L}$ syringe were dropped perpendicularly onto the membrane surface at room temperature. Each membrane was measured five times, and the mean value was recorded. The thermal properties of all samples were studied by DSC (DSC, PerkinElmer). In a nitrogen atmosphere, about 3–5 mg of sample was heated from $30\text{ }^\circ\text{C}$ to $250\text{ }^\circ\text{C}$ at a rate of $10\text{ }^\circ\text{C min}^{-1}$. Thermogravimetric measurement (TGA) was performed in dynamic mode using a TA instrument (Q500 thermal analyzer, TA) with nitrogen atmosphere (flow rate = 60 mL min^{-1}). The sample was under nitrogen atmosphere and heated from room temperature to $800\text{ }^\circ\text{C}$ ($10\text{ }^\circ\text{C min}^{-1}$).

2.3. Synthesis of monomer

D4, TMDS, and Kg-23 catalyst were placed in a three-neck flask, and the reaction was heated to $80\text{ }^\circ\text{C}$ under nitrogen atmosphere for 12 h. After purification, the viscous, transparent oil terminated hydrogen siloxane monomer was obtained and denoted as 2H-PDMS-10. Yield: about 86%. 1H NMR (600 MHz, Chloroform-*d*) δ 4.71 (m, 2H), 0.28 to -0.04 (m, 60H).

TMDS, dimethyldichlorosilane, and deionized water were added, and the solution was mixed for three days at room temperature. Then, the crude product was neutralized, dried, and distilled under reduced pressure. A colorless transparent liquid was obtained and denoted as TTDS. Yield: about 82%. As shown in Scheme 1. 1H NMR (600 MHz, Chloroform-*d*) δ 4.71 (m, 1H), 0.21 (m, 6H), 0.09 (m, 3H).

4,4'-Dihydroxydiphenyl, K_2CO_3 , and bromopropene were placed in a flask. The reaction was heated to $85\text{ }^\circ\text{C}$ for 8 h, and then a large amount of distilled water was added to the reaction to obtain white crystals, which were rinsed and dried. The dried product was followed to Claisen Rearrangement, which was heated at $205\text{ }^\circ\text{C}$ for 2 h under the protection

of nitrogen before recrystallizing with n-heptane to obtain the compound 3,3'-diallyl-4,4'-biphenol (DABP). 1H NMR (600 MHz, DMSO-*d*₆) δ 9.313 (m, 1H), 7.197 (m, 2H), 6.821 (m, 1H), 5.976 (m, 1H), 5.040 (m, 2H), 3.321 (m, 2H), as shown in Scheme 1.

2.4. Polymer synthesis

TMDS, TTDS, and 2H-PDMS-10 were placed three flasks. After adding excess DABP, they were heated to $110\text{ }^\circ\text{C}$ for 10 min. Then, $50\text{ }\mu\text{L}$ of Karstedt's catalyst was added, and the reaction was allowed to proceed for 10 h. To remove the toluene solvent and low-boiling-point copolymer, rotary evaporation was performed. Three DABP/PDMS copolymer samples with different segment ratios (hereafter denoted as DPn, where $n = 0, 1, \text{ and } 8$) were obtained, as shown in Scheme 2. 1H NMR as shown in Fig. S1.

DP0: 1H NMR (600 MHz, DMSO-*d*₆) δ 9.26–9.06 (m, 1H), 7.30–7.12 (m, 2H), 6.81 (m, 1H), 2.59–2.54 (m, 2H), 1.59 (m, 2H), 0.56 (m, 2H), 0.13 to -0.07 (m, 6H).

DP1: 1H NMR (600 MHz, Chloroform-*d*) δ 7.37–7.23 (m, 1H), 6.96 (m, 1H), 6.92–6.75 (m, 1H), 3.96 (m, 1H), 2.68 (m, 1H), 1.92–1.62 (m, 2H), 0.68 (m, 2H), 0.22 to -0.02 (m, 9H).

DP8: 1H NMR (600 MHz, Chloroform-*d*) δ 7.50–7.42 (m, 1H), 6.95 (m, 1H), 6.87–6.77 (m, 1H), 2.69 (m, 2H), 1.72 (m, 2H), 0.71–0.63 (m, 2H), 0.31 to -0.04 (m, 30H).

2.5. Membrane fabrication

To fabricate the copolymer that was used as the scaffold for the microsphere-coated membrane, a doping solution was prepared by adding 10% (w/v) PVDF into the mixed solvent with DMF and acetone (3:2, v/v), followed by stirring at room temperature for 6 h until the polymer was dissolved completely. Electrospun membranes were obtained through the accumulation of charged (16 kV) nanofibers on a collector (12 cm from the nozzle) at a flow rate of 0.5 mL/h. To form the surface structure of the two kinds of coated membranes with well-shaped polymer microspheres, 2% DPn with 2% PVDF (w/v) were mixed solvent with DMF and THF (3:2, v/v), which were electrospun to fabricate the hierarchical membrane. The electrospinning parameters were as follows: applied voltage of 16 kV, receiving distance of 12 cm, and feeding rate of 0.5 mL/h. The schematic of the electrospinning device is shown in Fig. 1. Finally, the fabricated double-layer membranes were carefully taken out of the barrel and dried in an oven at $50\text{ }^\circ\text{C}$ for more than 24 h. All membranes were fabricated at room temperature with relative humidity less than 50%.

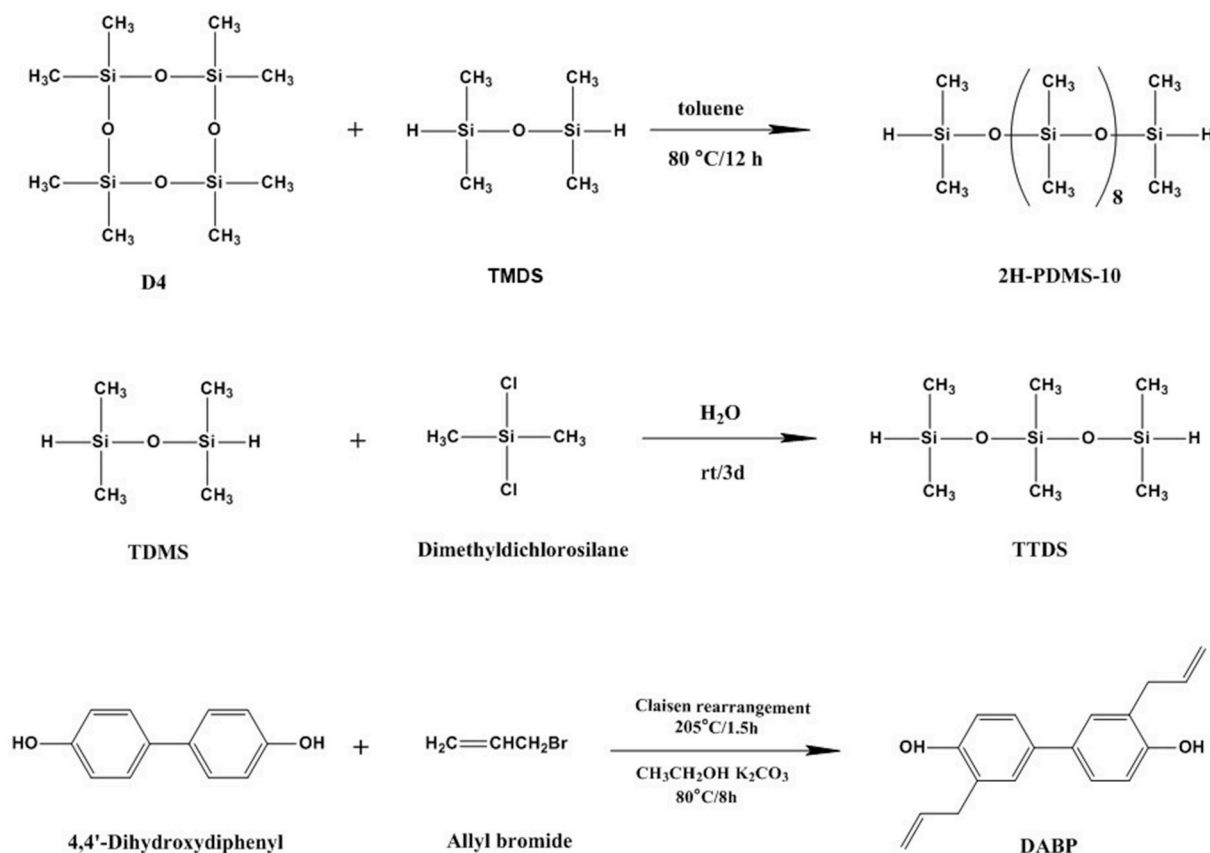
2.6. Oil–water separation

To measure the oil–water separation performance of PVDF/DPn membranes, they were fixed between a glass funnel and a beaker with an effective separation area of 4.41 cm^2 . To induce contact between the oil phase and membrane, the oil–water separation equipment was placed at an angle of 45° , and 30 mL of n-hexane mixed with 30 mL of water was poured into the upper glass funnel. Separation was achieved by gravity. To ensure completed separation, the system was maintained for 5–10 min, and then two barrels were used to collect oil and water. The calculation formula of separation efficiency was as follows:

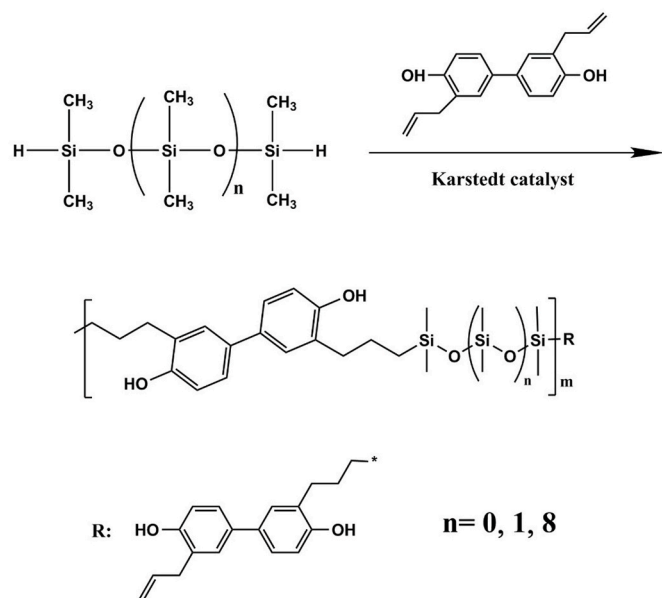
$$\phi = \frac{v_1}{v_2} \quad (1)$$

where ϕ is the separation efficiency, and v_1 and v_2 are the volume of oil before and after separation (mL), respectively. The calculation formula of oil–water separation flux was as follows:

$$Flux = \frac{V}{At} \quad (2)$$



Scheme 1. Synthesis of hydrogen-terminated siloxane and DABP.



Scheme 2. Synthesis of DABP/PDMS copolymer.

where V is the volume of oil phase passing through the membrane (L), A is the effective area of separation membrane (m^2), and t is the separation time (h).

3. Results and discussion

3.1. Synthesis of DPn copolymers

TTDS, 2H-PDMS-10, and DABP were synthesized by hydrolysis, cation ring opening, and Claisen rearrangement. Fig. 2b shows the ^1H NMR of DABP, with the integrals at 9.313, 7.197, 6.821, 5.976, 5.040, and 3.321 ppm. The intensity ratio was 1:2:1:1:2:2. Fig. 2c shows the ^1H NMR of TTDS, and the integrated intensity ratio at 4.74, 0.21, and 0.09 ppm was 1:6:3. For the ^1H NMR of 2H-PDMS-10, the integrated intensity ratio at 4.74 and 0.12 ppm was 2:60, as shown in Fig. 2d. The data and structure calculation formula well agreed. This finding showed that all polymer monomers were successfully synthesized.

Copolymers with different rigid-flexible segment ratios were synthesized by hydrosilylation. The FT-IR spectra of TMDS, TTDS, 2H-PDMS-10, DP0, DP1, and DP8 are illustrated in Fig. 2a. Signals at 1060 and 1250 cm^{-1} [31] for the Si-O-Si and Si-CH₃ bonds stretching in each spectrum demonstrated the same chemical composition of TMDS, TTDS, 2H-PDMS-10, DP0, DP1, and DP8. The infrared spectra show that TMDS, TTDS, and 2H-PDMS-10 had Si-H bond stretching vibration peaks at 2130 cm^{-1} [32], but the Si-H bond almost disappeared in DP0, DP1, and DP8 polymers possibly, which due to we added an excess of DABP. Therefore, the Si-H bond stretching vibration peak is almost invisible in the infrared spectra. To further prove the hydrosilylation between the monomers, we used liquid chromatography to determine the molecular weight of the polymers DP0, DP1, and DP8. We found that the molecular weights of the polymers were all around 10 000, further proving that the polymer was successfully synthesized.

3.2. Morphology and property of PVDF/DPn electrospinning membrane

SEM images in Fig. 3a-d showed the evolution of morphology of

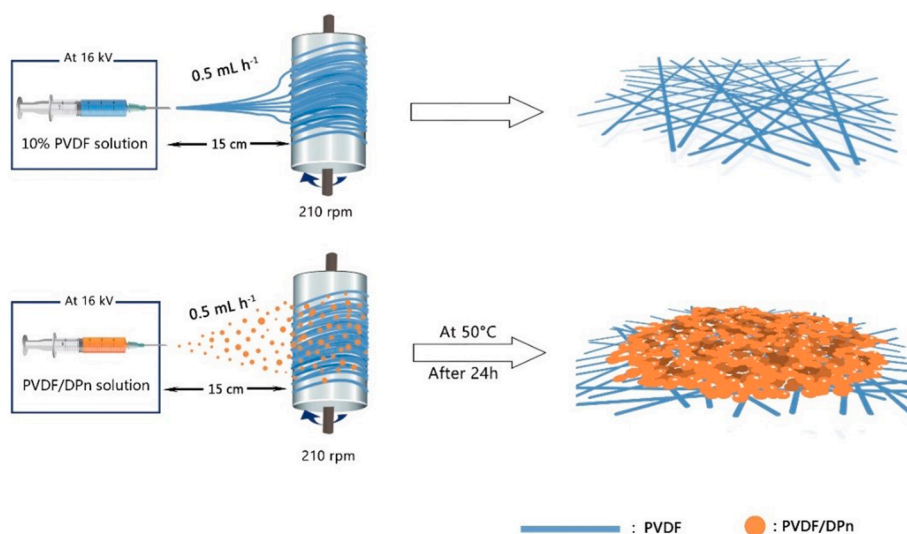


Fig. 1. Fabrication of polymeric-microsphere-coated membrane.

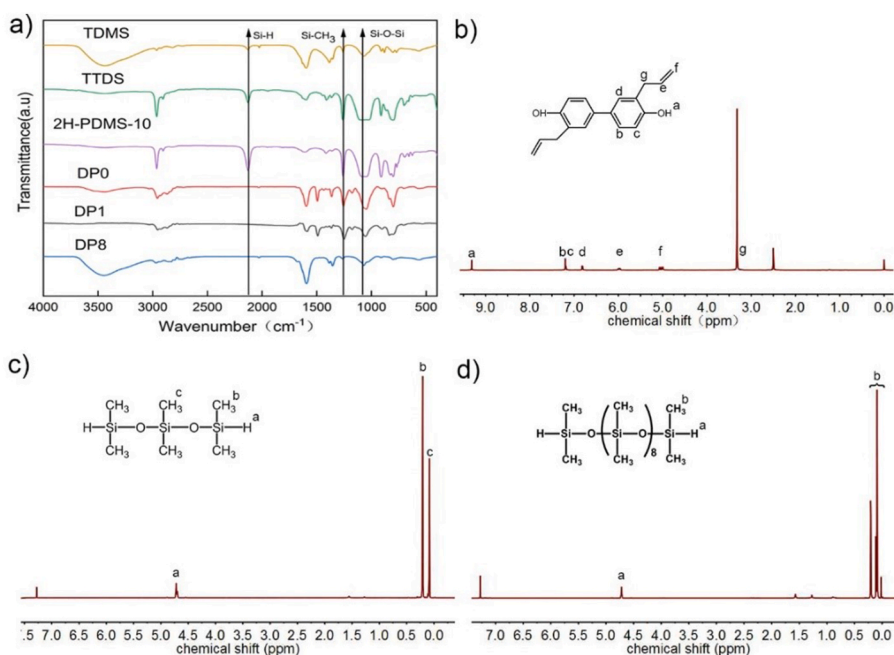


Fig. 2. FT-IR spectra of TDMS, TTDS, 2H-PDMS-10, DP0, DP1, and DP8 (a). ^1H NMR spectra of DABP, TTDS, and 2H-PDMS-10 (b–d).

electrospun PVDF and electrospayed PVDF/DPn on PVDF surface. The hierarchical structure is displayed in Fig. 3a₃, 3b₃, 3c₃ and 3d₃. The diameter of the electrospun PVDF nanofiber with an average fiber diameter (AFD) of 550 nm was relatively uniform; its surface was smooth and no obvious beaded structure existed at 10% PVDF concentration (Fig. 3a₁–3a₄). Electrospinning was determined by factors such as molecular weight and concentration. Owing to the low molecular weight of copolymer DPn ($M_w \approx 10\,000$), electrospinning or electrospaying cannot be carried out, so PVDF and DPn were mixed to form a spinning solution, and electrospinning was performed. High microsphere density and hierarchical structure are known to improve membrane hydrophobicity [33]. Accordingly, in the present study, 4% concentration of blended solution was selected for electrospaying onto the PVDF nanofiber membrane to form a hierarchical structure and thus improve membrane hydrophobicity (Fig. b₁–d₄). With increased n from 0 to 8, the average microsphere diameter (AMD) increased from 1.56 μm to 1.78 μm . This finding was primarily due to the increase in Si–O–Si

segments in the polymer, which enhanced the entanglement of PVDF and between DPn. Compared with a pure PVDF membrane, when a layer of microspheres was placed on the membrane surface (Fig. 3b₂), the surface roughness of membrane significantly increased. When $n = 0$, the polymer formed only smooth microspheres on the membrane surface (Fig. 3b₂). Interestingly, when n was increased to 1, honeycomb through-holes (Fig. 3c₁) obviously formed on the membrane surface. When $n = 8$, the structure of such through-holes became increasingly obvious (Fig. 3d₁). This finding could possibly be due to the process of electrospaying facilitating the formation of the through-hole-like structure owing to the attraction and repulsion of charged ions. We explain this phenomenon in detail in the next chapter. Additionally, element-mapping images (Fig. 4a) were obtained to examine the surface element composition of copolymer membranes; the mapped red, green, purple, and blue correspond to carbon, oxygen, fluorine, and silicon elements, respectively. These results showed that all elements were evenly distributed on the membrane surface. The FT-IR spectra of membranes are illustrated in Fig. 4b. In all

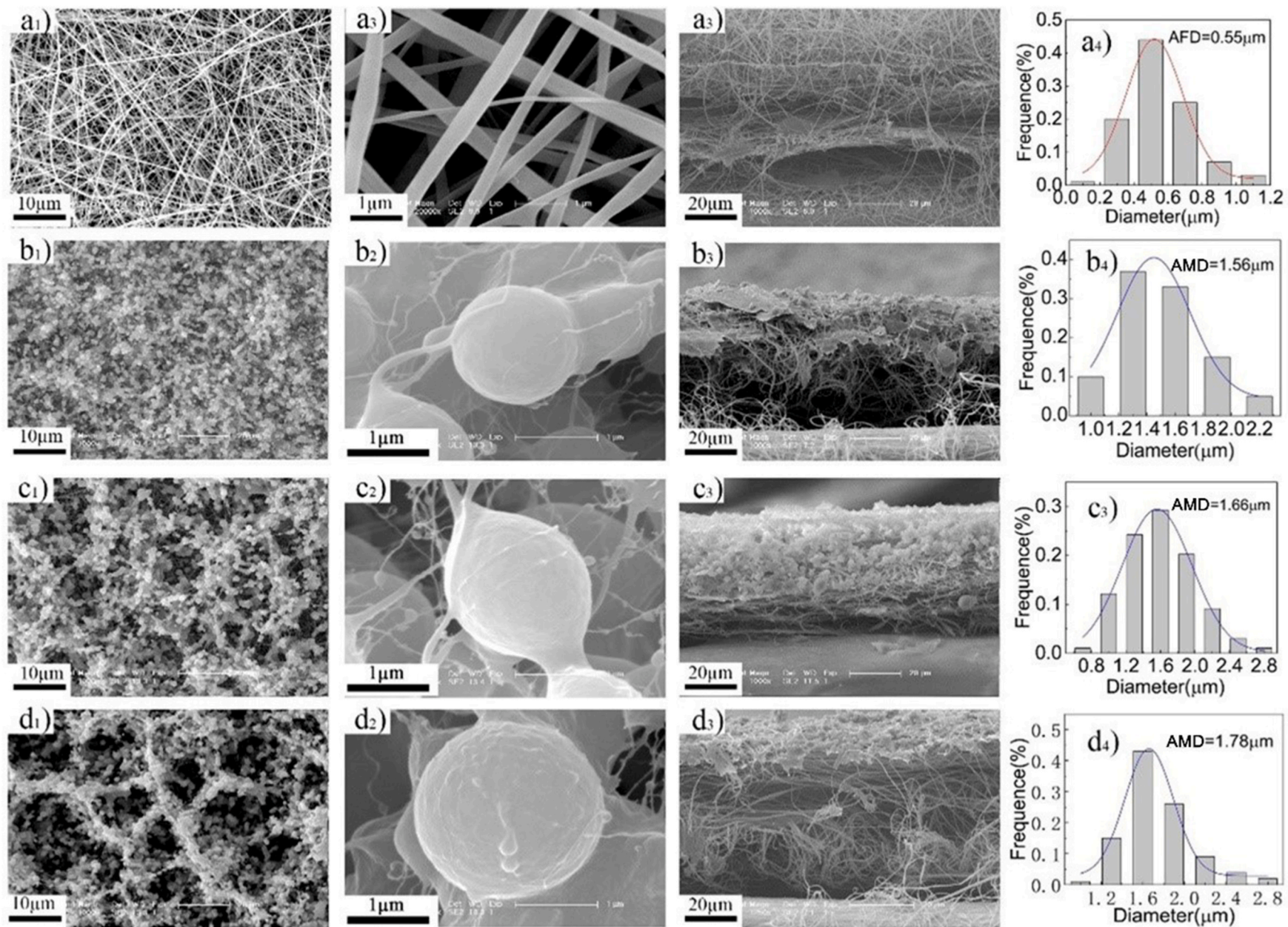


Fig. 3. Morphology and performance characterizations of composite membranes. (a₁–d₄) SEM images of diameter distributions; the top surface and cross-sections for pure PVDF membrane and DP0 to DP8 composite membranes.

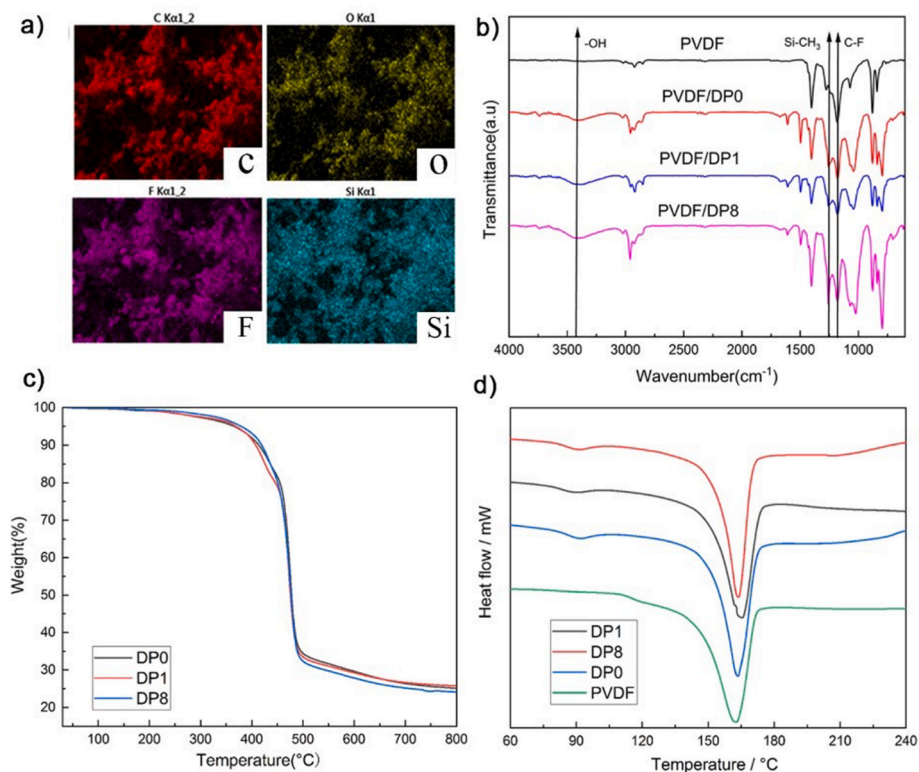


Fig. 4. (a) Mapping images of DP8 composite membrane with carbon (red), oxygen (green), fluorine (purple), and silicon (blue) elements. (b) FT-IR spectra of all of the membranes. (c) TGA and (d) DSC curves for pure PVDF membrane and DP0 to DP8 composites membrane. (For interpretation of the references to color in this figure legend, the reader is referred to the Web version of this article.)

the membrane, C–F symmetrical stretching vibrations appeared at the peak of 1168 cm^{-1} . This result was owing to the presence of PVDF in all membranes. However, peaks at 3470 and 1280 cm^{-1} attributed to $-\text{OH}$ vibration and $\text{Si}-\text{CH}_3$ were observed, further proving that PVDF and DPn were successfully compounded into the membrane. Based on the above analysis, the copolymer membrane was successfully fabricated by co-electrospinning DPn and PVDF.

The thermal stability of a membrane is crucial to its long-term stable use. Herein, thermal stability was analyzed by TGA and DSC under a nitrogen atmosphere, and the results are shown in Fig. 4c and d. All membranes began to degrade at about $400\text{ }^\circ\text{C}$; the weight-loss rate was about 76%, and the melting point was about $164\text{ }^\circ\text{C}$. This finding showed that when DPn was added to PVDF, the thermal performance of the membrane was not reduced.

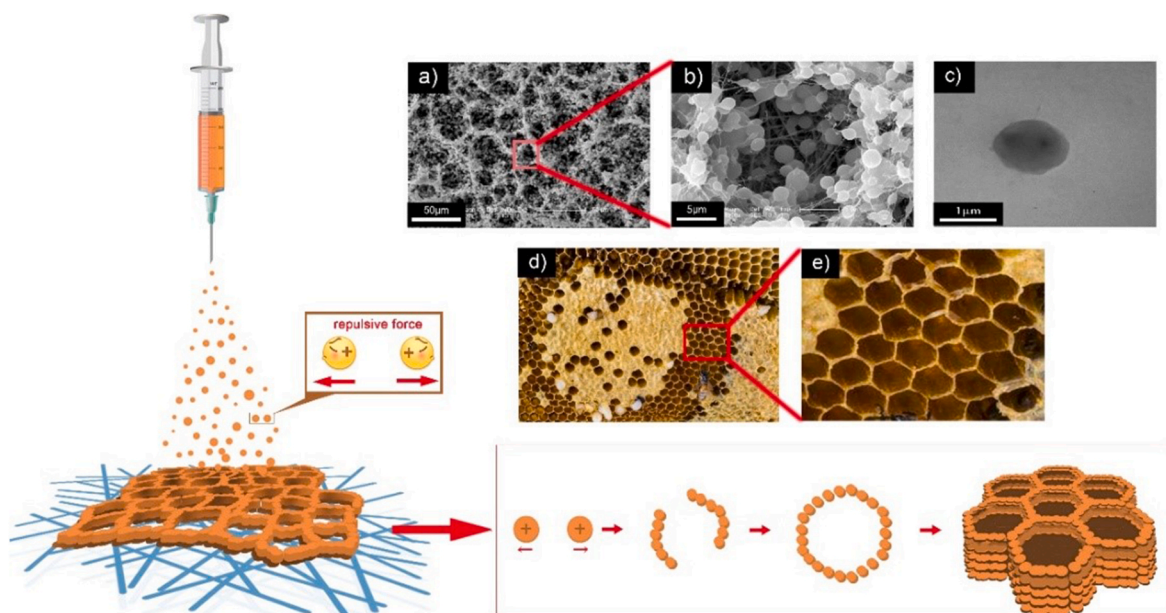


Fig. 5. Formation mechanism of honeycomb through-hole membrane. (a, b) SEM images of the surface of DP8 composite membrane. (c) TEM images of DP8 microspheres. (d, e) Photos of natural honeycomb.

3.3. Formation mechanism of the honeycombed through-hole structure

Fig. 5 shows the formation mechanism of honeycomb through-holes. Natural honeycombs showed a special structure with horizontal layered networks and vertical channels (Fig. 5d and e), which increased the rapid passage volume of liquid and benefited the oil–water separation owing to the bionic structure. The membrane surface presented a neatly arranged honeycomb grid structure (Fig. 5a). The magnified SEM image revealed solid microspheres (Fig. 5b and c) piled up in a single through-hole with a diameter of about 20 μm . Furthermore, the fiber structure of the bottom layer can be clearly observed, proving that a through-hole structure was formed. This finding was due to the phenolic hydroxyl group of DPn. The phenolic hydroxyl group itself can be ionized to increase the conductivity of the jet. The electrostatic repulsion of the non-solidified electrospun microspheres was significant during electrospinning, resulting in the formation of the honeycomb-like network structure. We proposed a simplified model to clarify the three-dimensional self-assembly mechanism of the PVDF/DPn multilayer honeycomb structure (Fig. 5). Microspheres with the same charge may drive by the electrostatic repulsion and deposit onto the PVDF surface at a certain distance from one another. The succeeding microspheres preferentially stacked on top of the deposited microspheres to form a through-hole structure. The microspheres deposited layer by layer to undergo rapid self-assembly via dissipation and minimize their energy [34,35]. Owing to superposition electrostatic repulsion, the honeycomb structure was obtained accordingly.

3.4. Oil–water separation

Membrane hydrophobicity is an important determinant of the efficiency of oil–water separation. Fig. 6b shows the WCAs of pure PVDF nanofiber membrane and P-DPn composite membranes. The hydrophobic angle of pure PVDF nanofiber membrane was only $121.9^\circ \pm 0.7^\circ$. When the microspheres formed by the mixture of PVDF and DPn sprayed onto the PVDF nanofiber membrane, the WCA values of the polymer membrane were $138.3^\circ \pm 0.6^\circ$, $140.0^\circ \pm 0.3^\circ$, and $145.3^\circ \pm 0.8^\circ$, respectively. They were all higher than that of pure PVDF membrane primarily because the surface energy of PDMS was lower than that of PVDF. Additionally, the introduction of microspheres led to increased surface roughness. The membrane surface formed a microprotruding structure that trapped air on the membrane surface. It formed a thin air layer between the liquid droplet and solid surface, reducing the interaction force between the solid surface and droplet, so the droplet can easily slide onto the solid surface without being wetted. Consequently, surface hydrophobicity increased (Fig. 7e and f). Interestingly, with increased n in the polymer DPn segment from 0 to 8, the hydrophobic angle increased. This finding was due to the increase in the hydrophobic group (Si–CH₃) in the flexible segment PDMS leading to an increase in the hydrophobic angle.

Based on the hydrophobic properties, PVDF and DPn membranes were used to separate the stratified oil–water mixture. The oil–water separation system was operated solely by gravity drive, as shown in Fig. 6a. About 60 mL of liquid mixture containing 30 mL of water (dyed

with methyl blue) and 30 mL of n-hexane (dyed with Sudan III) were placed in a 100 mL beaker. To allow the film to sufficiently make contact with the oil phase, we tilted the separation device by 45° . Then, 60 mL of the oil–water mixture was poured into the upper funnel, the membranes were quickly wetted, and the oil passed through the membranes into the beaker. Meanwhile, the water was blocked into the funnel, and almost no residual oil remained in the water after separation. Fig. 7a shows the oil–water separation flux. The oil flux of pure PVDF membrane was only about $2000 \text{ L m}^{-2} \text{ h}^{-1}$, but the flux of the DPn layered membranes was $>4500 \text{ L m}^{-2} \text{ h}^{-1}$. With increased n , the flux of oil–water separation significantly increased, corresponding to our previous SEM results (Fig. 2b₁, 2c₁, and 2d₁), which was owing to the formation of a hierarchical structure and the formation of a through-hole after a layer of microspheres were placed on the nanofiber membrane. Fig. 7b shows the oil–water separation efficiency, which all remained above 99.80%. The separation efficiency of DPn membranes with a layered microsphere structure was also higher than that of pure PVDF membrane. For all the oil–water mixtures separated in this study, the flux and separation efficiency for each oil was calculated up to more than $4200 \text{ L m}^{-2} \text{ h}^{-1}$ and 99.80%, as shown in Fig. 7c and d, which is significantly higher than pure PVDF membrane. As shown in Table 1, it can be concluded that the DPn membrane exhibited the fastest permeate flux and highest separation efficiency to separate oil–water mixtures compared to other literature reports [36–39]. Finally, in order to further test the oil–water separation performance of the membrane, 3 mL water and 30 mL oil (n-hexane) were mixed, and then 2 mg the surfactant (Tween-80) was added into the mixture solution by stirring for 6h. The diameter range of droplets observed was 1–4 μm under the optical microscopy observation (Carl Zeiss-axio Image A2m, Germany), as shown in Fig. S2. Fig. S2 showed the comparison between the water-in-oil emulsion (left) and the collected filtrate (right). Fig. S3a and b shown the oil flux of the DP8 membrane can achieve above $205 \text{ L m}^{-2} \text{ h}^{-1}$ and the separation efficiency was above 95%, which indicated that the water droplets were effectively cut off and the water-in-oil emulsion was effectively separated by the electrospun membrane.

According to Wenzel's [40] and Cassie's [16] surface wettability principle, the surface chemical structure and geometry are the main factors affecting the surface contact angle of the membrane. Based on this theory, the layered-structure composite membrane prepared by electrospinning PVDF/DPn copolymer had an ideal geometry. The microspheres on the surface mimicked the microconvex structure of the lotus leaf. The hydrophobicity of DPn with lower surface energy was greatly enhanced on the surface of PVDF membrane (Fig. 7e and f). At the same time, air pockets were introduced between the solid and liquid, and these air pockets dragged the droplets up, which was conducive to the formation of hydrophobic surfaces. Therefore, the PVDF/DPn membrane had ultrahigh separation efficiency and good separation flux for oil–water mixtures.

4. Conclusions

Biomimetic hydrophobic membranes with layered microsphere structure were successfully prepared by electrospinning and

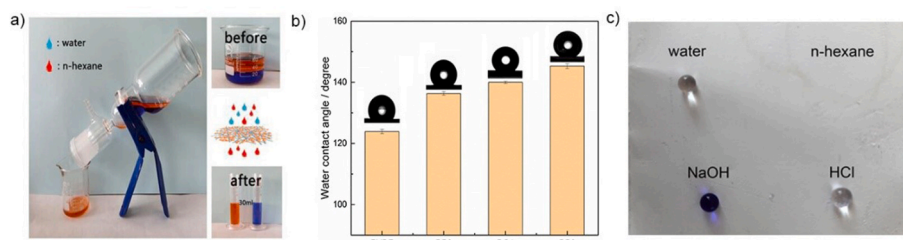


Fig. 6. (a) Photographs for n-hexane–water separation. (b) Comparison of WCA values between pure PVDF membrane and DPn composite membranes. (c) Deionized water, 2 M NaOH, 2 M HCl sitting on the surface while oil (n-hexane) droplet spreading and penetrating through the fibrous membrane.

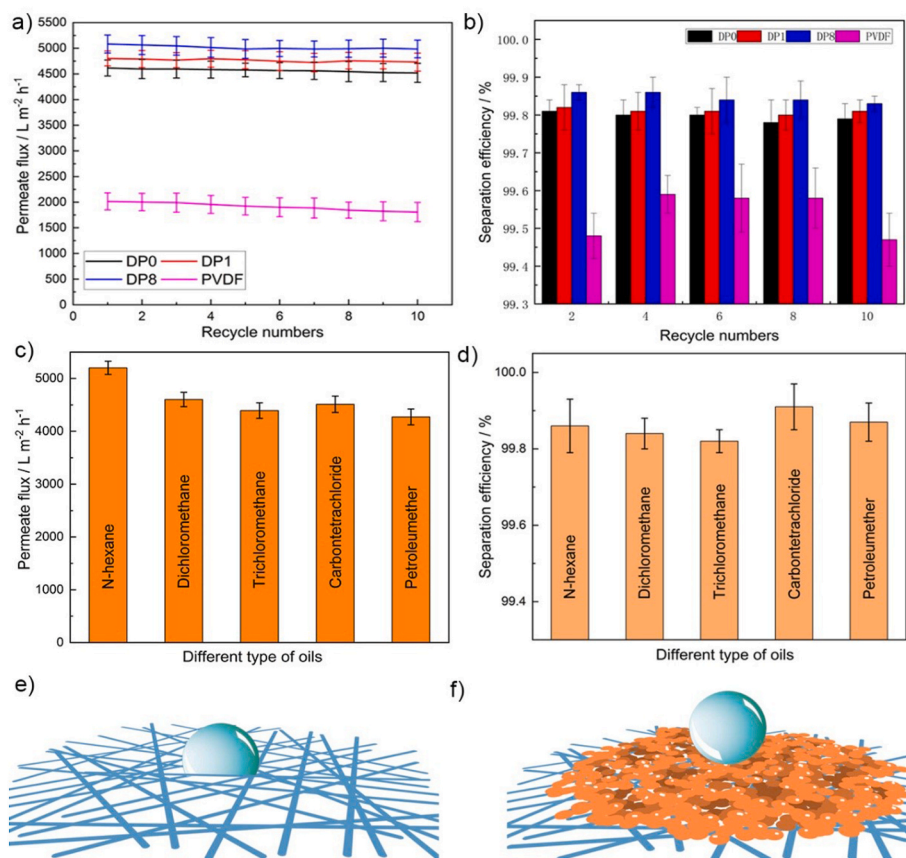


Fig. 7. Oil–water separation with different cycles by using the PVDF, DP0, DP1, and DP8 membranes: (a) n-hexane flux, and (c) separation efficiency. Flux (c) and separation efficiency (d) of various mixtures through DP8 membrane. (e) Hydrophobic mechanism of pure PVDF membrane surface. (f) Electro-spray-coated hydrophobic membrane with irregular beads on the surface.

Table 1

Comparison of the permeate fluxes ($L m^{-2} h^{-1}$) and efficiencies (%) of various membranes.

Segregator	Permeate flux ($L m^{-2} h^{-1}$)	Separation efficiency (%)	Ref.
PVDF/SiO ₂ microspheres coating	1500 to 2050	97.5	37
Cu(OH) ₂ nanoneedles mesh	1980	97.0	38
Copper-coated meshes	110 to 569	97.0	39
Novel foam membranes (FMs)	300 to 500	98.0	40
DPn membrane	4200	99.8	This study

electrospraying. The copolymer DPn with different rigid–flexible segment ratios was successfully prepared by hydrosilylation. Hereafter, it was mixed with PVDF to successfully form microspheres on the surface of PVDF fiber mat. After adding DPn to PVDF, the melting point and degradation temperature of the film remained at around 164 °C and 400 °C, indicating that the thermal stability of the film had not changed significantly. In the process of electro-spraying, the through-hole structure was formed owing to the electrostatic repulsion caused by the charge of the microspheres, which benefited the separation of oil and water. Moreover, all DPn membranes had outstanding hydrophobicity and could be applied to oil–water separation considering their excellent separation efficiency and reusability. Moreover, after 10 cycles of oil–water separation test, the copolymer membrane retained its excellent separation efficiency (>99.80%) and flux. Overall, we synthesized herein a PDMS membrane with rigid segments, and this structure can

form honeycomb through holes in the process of electro-spraying. Flux and separation efficiency were improved, thereby providing a new method of increasing the flux of oil–water separation.

CRediT authorship contribution statement

Shuai Luo: Conceptualization, Methodology, Investigation, Writing - original draft. **Xueyan Dai:** Methodology, Investigation, Writing - review & editing. **Yanlong Sui:** Methodology, Investigation, Writing - review & editing. **Peihong Li:** Writing - review & editing. **Chunling Zhang:** Funding acquisition, Supervision, Project administration, Writing - review & editing.

Declaration of competing interest

The authors declare that they have no known competing financial interests or personal relationships that could have appeared to influence the work reported in this paper.

Acknowledgements

The authors gratefully acknowledge the financial supports for this research from the National Natural Science Foundation of China (No. 52073112), the Natural Science Foundation of Jilin Province (No. 20180101197jc), and the International Science and Technology Cooperation Program of China (No. 20190701001GH).

Appendix A. Supplementary data

Supplementary data to this article can be found online at <https://doi.org/10.1016/j.polymer.2021.123522>.

[org/10.1016/j.polymer.2021.123522](https://doi.org/10.1016/j.polymer.2021.123522).

References

- [1] F. Ahmed, S. Saleemi, Z. Khatri, M.I. Abro, I.S. Kim, Co-electrospun poly(ϵ -caprolactone)/cellulose nanofibers-fabrication and characterization, *Carbohydr. Polym.* 115 (2015) 388–393, <https://doi.org/10.1016/j.carbpol.2014.09.002>.
- [2] H.F. Alotaibi, Y. Al Thaher, S. Perni, P. Prokopovich, Role of processing parameters on surface and wetting properties controlling the behaviour of layer-by-layer coated nanoparticles, *Curr. Opin. Colloid Interface Sci.* 36 (2018) 130–142, <https://doi.org/10.1016/j.cocis.2018.02.008>.
- [3] A. Jernelv, The threats from oil spills: now, then, and in the future, *Ambio* 39 (2010) 353–366, <https://doi.org/10.1007/s13280-010-0085-5>.
- [4] Z. Chu, Y. Feng, S. Seeger, Oil/water separation with selective superantwetting/superwetting surface materials, *Angew. Chem. Int. Ed.* 54 (2015) 2328–2338, <https://doi.org/10.1002/anie.201405785>.
- [5] R.P.J. Swannell, K. Lee, M. McDonagh, Field evaluations of marine oil spill bioremediation, *Microbiol. Rev.* 60 (1996) 342–365, <https://doi.org/10.1128/mmr.60.2.342-365.1996>.
- [6] N.P. Ventikos, E. Vergetis, H.N. Psarftas, G. Triantafyllou, A high-level synthesis of oil spill response equipment and countermeasures, *J. Hazard Mater.* 107 (2004) 51–58, <https://doi.org/10.1016/j.jhazmat.2003.11.009>.
- [7] V. Broje, A.A. Keller, Improved mechanical oil spill recovery using an optimized geometry for the skimmer surface, *Environ. Sci. Technol.* 40 (2006) 7914–7918, <https://doi.org/10.1021/es061842m>.
- [8] Q. Zhu, Q. Pan, F. Liu, Facile removal and collection of oils from water surfaces through superhydrophobic and superoleophilic sponges, *J. Phys. Chem. C* 115 (2011) 17464–17470, <https://doi.org/10.1021/jp2043027>.
- [9] H. Bi, X. Xie, K. Yin, Y. Zhou, S. Wan, L. He, F. Xu, F. Banhart, L. Sun, R.S. Ruoff, Spongy graphene as a highly efficient and recyclable sorbent for oils and organic solvents, *Adv. Funct. Mater.* 22 (2012) 4421–4425, <https://doi.org/10.1002/adfm.201200888>.
- [10] Y. Zhu, D. Wang, L. Jiang, J. Jin, Recent progress in developing advanced membranes for emulsified oil/water separation, *NPG Asia Mater.* 6 (2014), <https://doi.org/10.1038/am.2014.23>.
- [11] I. Sadeghi, A. Aroujalian, A. Raisi, B. Dabir, M. Fathizadeh, Surface modification of polyethersulfone ultrafiltration membranes by corona air plasma for separation of oil/water emulsions, *J. Membr. Sci.* 430 (2013) 24–36, <https://doi.org/10.1016/j.memsci.2012.11.051>.
- [12] I. Sadeghi, P. Kaner, A. Asatekin, Controlling and expanding the selectivity of filtration membranes, *Chem. Mater.* 30 (2018) 7328–7354, <https://doi.org/10.1021/acs.chemmater.8b03334>.
- [13] R.N. Wenzel, Surface roughness and contact angle, *J. Phys. Colloid Chem.* 53 (1949) 1466–1467, <https://doi.org/10.1021/j150474a015>.
- [14] H. Bellanger, T. Darmanin, E. Taffin De Givenchy, F. Guittard, Chemical and physical pathways for the preparation of superoleophobic surfaces and related wetting theories, *Chem. Rev.* 114 (2014) 2694–2716, <https://doi.org/10.1021/cr400169m>.
- [15] T. Darmanin, F. Guittard, Recent advances in the potential applications of bioinspired superhydrophobic materials, *J. Mater. Chem. A* 2 (2014) 16319–16359, <https://doi.org/10.1039/c4ta02071e>.
- [16] H.J. Ensikat, P. Ditsche-Kuru, C. Neinhuis, W. Barthlott, Superhydrophobicity in perfection: the outstanding properties of the lotus leaf, *Beilstein J. Nanotechnol.* 2 (2011) 152–161, <https://doi.org/10.3762/bjnano.2.19>.
- [17] F. Zhang, B.W. Robinson, H. De Villiers-Lovelock, R.J.K. Wood, S.C. Wang, Wettability of hierarchically-textured ceramic coatings produced by suspension HVOF spraying, *J. Mater. Chem. A* 3 (2015) 13864–13873, <https://doi.org/10.1039/c5ta02130h>.
- [18] X. Su, H. Li, X. Lai, Z. Yang, Z. Chen, W. Wu, X. Zeng, Vacuum-assisted layer-by-layer superhydrophobic carbon nanotube films with electrothermal and photothermal effects for deicing and controllable manipulation, *J. Mater. Chem. A* 6 (2018) 16910–16919, <https://doi.org/10.1039/c8ta05273e>.
- [19] P. Xu, T.W. Coyle, L. Pershin, J. Mostaghimi, Superhydrophobic ceramic coating: fabrication by solution precursor plasma spray and investigation of wetting behavior, *J. Colloid Interface Sci.* 523 (2018) 35–44, <https://doi.org/10.1016/j.jcis.2018.03.018>.
- [20] M. Yang, W. Liu, C. Jiang, S. He, Y. Xie, Z. Wang, Fabrication of superhydrophobic cotton fabric with fluorinated TiO₂ sol by a green and one-step sol-gel process, *Carbohydr. Polym.* 197 (2018) 75–82, <https://doi.org/10.1016/j.carbpol.2018.05.075>.
- [21] B. Satilmis, T. Uyar, Superhydrophobic hexamethylene diisocyanate modified hydrolyzed polymers of intrinsic microporosity electrospun ultrafine fibrous membrane for the adsorption of organic compounds and oil/water separation, *ACS Appl. Nano Mater.* 1 (2018) 1631–1640, <https://doi.org/10.1021/acsnano.8b00115>.
- [22] C. Zhang, P. Li, B. Cao, Electrospun microfibrillar membranes based on PIM-1/POSS with high oil wettability for separation of oil-water mixtures and cleanup of oil soluble contaminants, *Ind. Eng. Chem. Res.* 54 (2015) 8772–8781, <https://doi.org/10.1021/acs.iecr.5b02321>.
- [23] Y. Huang, C. Xiao, Q. Huang, H. Liu, Z. Guo, K. Sun, Robust preparation of tubular PTFE/FEP ultrafine fibers-covered porous membrane by electrospinning for continuous highly effective oil/water separation, *J. Membr. Sci.* 568 (2018) 87–96, <https://doi.org/10.1016/j.memsci.2018.09.062>.
- [24] J. Gao, B. Li, L. Wang, X. Huang, H. Xue, Flexible membranes with a hierarchical nanofiber/microsphere structure for oil adsorption and oil/water separation, *J. Ind. Eng. Chem.* 68 (2018) 416–424, <https://doi.org/10.1016/j.jiec.2018.09.001>.
- [25] J. Ge, J. Zhang, F. Wang, Z. Li, J. Yu, B. Ding, Superhydrophilic and underwater superoleophobic nanofibrous membrane with hierarchical structured skin for effective oil-in-water emulsion separation, *J. Mater. Chem. A* 5 (2017) 497–502, <https://doi.org/10.1039/c6ta07652a>.
- [26] C. Yang, X.M. Li, J. Gilron, D. Feng Kong, Y. Yin, Y. Oren, C. Linder, T. He, CF₄ plasma-modified superhydrophobic PVDF membranes for direct contact membrane distillation, *J. Membr. Sci.* 456 (2014) 155–161, <https://doi.org/10.1016/j.memsci.2014.01.013>.
- [27] A.A. Rand, S.A. Mabury, Is there a human health risk associated with indirect exposure to perfluoroalkyl carboxylates (PFCA)s? *Toxicology* 375 (2017) 28–36, <https://doi.org/10.1016/j.tox.2016.11.011>.
- [28] P. Zhao, X. Xia, J. Dong, N. Xia, X. Jiang, Y. Li, Y. Zhu, Short- and long-chain perfluoroalkyl substances in the water, suspended particulate matter, and surface sediment of a turbid river, *Sci. Total Environ.* 568 (2016) 57–65, <https://doi.org/10.1016/j.scitotenv.2016.05.221>.
- [29] A. Tropmann, L. Tanguy, P. Koltay, R. Zengerle, L. Riegger, Completely superhydrophobic PDMS surfaces for microfluidics, *Langmuir* 28 (2012) 8292–8295, <https://doi.org/10.1021/la301283m>.
- [30] E.J. Park, Y.K. Cho, D.H. Kim, M.G. Jeong, Y.H. Kim, Y.D. Kim, Hydrophobic polydimethylsiloxane (PDMS) coating of mesoporous silica and its use as a preconcentrating agent of gas analytes, *Langmuir* 30 (2014) 10256–10262, <https://doi.org/10.1021/la502915r>.
- [31] E.J. Lee, B.J. Deka, J. Guo, Y.C. Woo, H.K. Shon, A.K. An, Engineering the Re-entrant hierarchy and surface energy of PDMS-PVDF membrane for membrane distillation using a facile and benign microsphere coating, *Environ. Sci. Technol.* 51 (2017) 10117–10126, <https://doi.org/10.1021/acs.est.7b01108>.
- [32] W. Jia, J.A. Kharraz, P.J. Choi, J. Guo, B.J. Deka, A.K. An, Superhydrophobic membrane by hierarchically structured PDMS-POSS electrocoat coating with cauliflower-shaped beads for enhanced MD performance, *J. Membr. Sci.* 597 (2020) 117638, <https://doi.org/10.1016/j.memsci.2019.117638>.
- [33] J. Wu, Y. Ding, J. Wang, T. Li, H. Lin, J. Wang, F. Liu, Facile fabrication of nanofiber- and micro/nanosphere-coordinated PVDF membrane with ultrahigh permeability of viscous water-in-oil emulsions, *J. Mater. Chem. A* 6 (2018) 7014–7020, <https://doi.org/10.1039/c8ta01539b>.
- [34] Y. Zhang, L. Wu, X. Wang, J. Yu, B. Ding, Super hygroscopic nanofibrous membrane-based moisture pump for solar-driven indoor dehumidification, *Nat. Commun.* 11 (2020) 1–11, <https://doi.org/10.1038/s41467-020-17118-3>.
- [35] S. Zhang, H. Liu, N. Tang, J. Ge, J. Yu, B. Ding, Publisher Correction: direct electrospinning of high-performance membranes based on self-assembled 2D nanoarchitected networks, *Nat. Commun.* 10 (1) (2019) 41467, <https://doi.org/10.1038/s41467-020-14864-2>, (1458), 10.1038/s41467-019-09444-y), *Nat. Commun.* 11 (2020).
- [36] J. Gao, X. Huang, H. Xue, L. Tang, R.K.Y. Li, Facile preparation of hybrid microspheres for super-hydrophobic coating and oil-water separation, *Chem. Eng. J.* 326 (2017) 443–453, <https://doi.org/10.1016/j.cej.2017.05.175>.
- [37] J. Liu, L. Wang, N. Wang, F. Guo, L. Hou, Y. Chen, J. Liu, Y. Zhao, L. Jiang, A robust Cu(OH)₂Nanoneedles mesh with tunable wettability for nonaqueous multiphase liquid separation, *Small* 13 (2017) 1–7, <https://doi.org/10.1002/sml.201600499>.
- [38] Z. Zhao, Y. Shen, H. Yang, J. Li, L. Guo, Underliquid superoleophobic copper-coated meshes for the separation of immiscible organic liquid mixtures, *ACS Appl. Mater. Interfaces* 11 (2019) 28370–28376, <https://doi.org/10.1021/acsami.9b05812>.
- [39] J.P. Chaudhary, S.K. Nataraj, A. Gogda, R. Meena, Bio-based superhydrophilic foam membranes for sustainable oil-water separation, *Green Chem.* 16 (2014) 4552–4558, <https://doi.org/10.1039/c4gc01070a>.
- [40] G. Wen, Z. Guo, W. Liu, Biomimetic polymeric superhydrophobic surfaces and nanostructures: from fabrication to applications, *Nanoscale* 9 (2017) 3338–3366, <https://doi.org/10.1039/c7nr00096k>.